



Hybrid photonic-plasmonic platform for high-throughput single-molecule studies

MINA MOSSAYEBI,¹ ALBERTO PARINI,² AMANDA J. WRIGHT,¹ MIKE G. SOMEKH,^{1,3} GAETANO BELLANCA,² AND ERIC C. LARKINS^{1,*}

¹Department of Electrical and Electronic Engineering, University of Nottingham, Nottingham, NG7 2RD, UK

²Department of Engineering, University of Ferrara, Ferrara, 44121, Italy

³Nanophotonics Research Centre, Shenzhen University, Shenzhen, PRC, 518060, China

*eric.larkins@nottingham.ac.uk

Abstract: We present the design and numerical characterization of a hybrid photonic-plasmonic nanoresonator comprised of a 2D photonic crystal (PhC) cavity, a gold bowtie nanoantenna (BNA) and a silicon dioxide, SiO₂, spacer. This device is designed to serve as the building block of a multicomponent platform capable of running multiple single-molecule experiments such as optical trapping and sample interrogation simultaneously. The thickness and structure of the spacer layer are adjusted to maximize the energy in the externally accessible hot-spot in the BNA gap. Suitability of the device for photonic integration is demonstrated by exciting it through a PhC waveguide.

Published by The Optical Society under the terms of the [Creative Commons Attribution 4.0 License](#). Further distribution of this work must maintain attribution to the author(s) and the published article's title, journal citation, and DOI.

1. Introduction

In biophotonics, there has been a drive over the last few decades to develop high-throughput, single cell/molecule techniques that avoid the pitfalls of bulk-averaged measurements. Optical techniques, such as trapping, manipulation, sensing and spectroscopy have received considerable attention, since they are minimally-invasive, often label-free and have the potential to be reconfigured in real time giving flexible positional control of the cell or molecule of interest [1]. Whilst techniques such as optical trapping are single-cell, they are not high-throughput and often require lengthy experiments on many individual cells before reliable conclusions can be reached [2]. These techniques typically operate on the micrometer scale. There is also a need to push them to the nanometer scale to make single molecule experiments possible. Finally, integrated solutions are needed to remove the barriers to the clinical uptake of single-cell/molecule technologies created by the need for highly trained users, long repetitive measurements and large, high-cost optical systems.

Photonic integrated circuits with hybrid photonic-plasmonic nanocavities are a promising new technology for future high-throughput single-molecule experiments. Devices for these applications require externally accessible regions of high optical power densities and low power dissipation translating into a need for optical cavities with a high-energy storage capacity and strong external spatial localization. The energy efficiency or resonant enhancement of the energy storage capacity of the optical cavity is described by the quality

factor, $Q = 2\pi \frac{\text{energy stored}}{\text{energy lost per cycle}}$. The effective mode volume, V_{eff} , described by

Kristensen *et al.* [3] is a commonly used measure of spatial energy localization. While V_{eff} is a well-established figure of merit for simple resonators, it can give anomalous values of mode volume for complex resonators where, for example, the confined light is coupled to a smaller externally accessible hot-spot. The challenge is to design a resonator with both a high Q and an externally accessible, nanoscale hot-spot for optical trapping and interrogation of single

molecules. This is driving the development of a new breed of hybrid photonic-plasmonic nanocavities and for this a different figure of merit will be introduced,

Plasmonic nanoantennas are able to localize light in regions a few tens of nanometers across, an order of magnitude smaller than the diffraction limit ($\sim \frac{0.6\lambda}{n_{eff}}$), where λ is wavelength of light and n_{eff} is the effective refractive index [4]. However, plasmonic devices

usually suffer from low resonant energy enhancement ($Q < 100$) due to radiation and absorption losses in the metal. Bowtie nanoantennas (BNAs) formed by placing two nanosized metallic triangles together with a narrow gap have been used in plasmonic nanotweezers [5–7], spectroscopy [8] and biosensing [9]. Nanoapertures in metal films have also been used for surface induced back action optical trapping of nanoparticles [10] and the trapping and unfolding of single proteins [11].

Photonic crystal (PhC) cavities, on the other hand, are extremely energy efficient and can achieve very high resonant enhancements ($Q > 100,000$) [12], but their spatial localization is limited by diffraction, with V_{eff} of the order of the cubic wavelength. Unfortunately, the very high intensity light in PhC structures is either confined within the dielectric material or in the holes or gaps in the dielectric structure. Thus, the hot-spots are either inaccessible for optical trapping or draw particles onto or inside the structure where they can adhere to the surface and become stuck.

This work designs a hybrid photonic-plasmonic resonator with both a high Q and an externally accessible, nanoscale optical hot-spot. This hybrid resonator represents a key building block that can be replicated many times to produce a multicomponent platform for high-throughput single-molecule experiments. This hybrid resonator is formed by combining a 2D PhC cavity, to provide an energy reservoir, with a BNA, to create an externally accessible nanoscale hot-spot. A dielectric spacer is placed between the PhC cavity and the BNA. The thickness and structure of the spacer controls the balance between Q of the cavity and the intensity in the external hot-spot. The resonant wavelength of these devices can be individually tuned by small changes to the PhC cavity. The inclusion of a PhC waveguide allows both fiber-optic coupling and the integration of hybrid resonator arrays for parallel trapping and interrogation. For arrays, the 2D photonic bandgap suppresses optical cross-talk between nearby devices.

This device builds on previous work combining PhC and plasmonic structures [13–38]. For example, C. Ciminelli, *et al.* (2014) designed and simulated a hybrid device based on a 1D PhC cavity coupled to a BNA [39]. They used a spacer block directly underneath the BNA, which hence only covered a small area of the 1D PhC. This device achieved high localization of light, but had a highly structured surface with etched features and holes, which may affect its future experimental performance. In our proposed device, the spacer layer covers the entire top surface of the device, not only the area underneath the BNA. The flat surface and compatibility with fiber optics make it practical for use in the life science applications.

2. The proposed hybrid device

The PhC cavity is based on a 275 nm thick gallium arsenide (GaAs) slab with a triangular lattice of air holes with periodicity, $a = 410$ nm, to form an air-suspended PhC membrane. An L3 cavity is formed by removing three adjacent holes from the PhC structure. The holes at the ends of the cavity are shifted by $0.2a$ outwards to increase the Q of the cavity [40]. GaAs was chosen due to its high refractive index resulting in high confinement of light in the vertical direction, but silicon and indium phosphide are also suitable. The L3 cavity is designed to operate in the 1530 - 1565 nm wavelength range to take advantage of well-established telecom technologies (e.g. photonic integrated circuits tunable lasers, fiber-optic components and test equipment).

The gold BNA consists of two 40 nm thick isosceles triangles forming a bowtie shape with a gap of 30 nm (the distance between the two tips), compatible with current fabrication procedures. The tip full-angle of each triangle, θ , is 30° and the total length of the BNA is 700 nm, also resulting in a resonance in the 1530 - 1565 nm range [41,42]. A SiO_2 spacing layer with a thickness, d , separates the PhC from the BNA. Its thickness can be adjusted to control the flow of energy between the PhC cavity and the BNA. The holes of the PhC membrane can be extended through the spacer layer to increase the Q of the device by reducing optical leakage in this layer. The BNA is positioned on top of the SiO_2 spacer at the center of the L3 cavity and oriented along the minor cavity axis (Fig. 1(a)), so that it couples to the central maximum of the fundamental TE mode of the cavity.

The device can be efficiently excited (and interrogated) via a W1 PhC waveguide, making it well suited for integration. The W1 PhC waveguide is created by removing a line of holes along the x direction as shown in Fig. 1(b). The waveguide design and distance from the waveguide to the cavity can be altered to control coupling to the cavity and maintain the high Q of the hybrid resonator, as described by S. Malaguti, *et al.* [43].

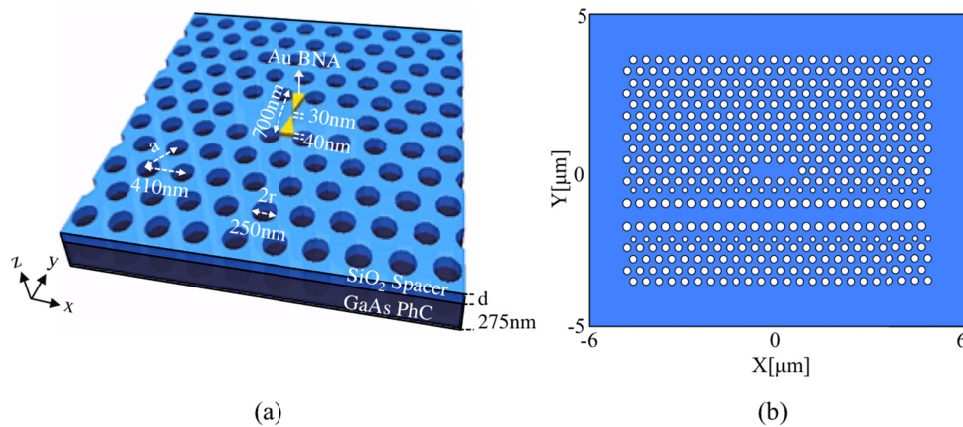


Fig. 1. (a) Illustration of the proposed hybrid device comprised of an L3 PhC cavity (black), a gold BNA (yellow) and a SiO_2 layer of thickness d (blue) and (b) an illustration of the W1 PhC waveguide used to excite the hybrid structure.

3. Simulation method

The results presented in this paper were obtained using a commercial-grade simulator based on the 3D finite difference time domain (FDTD) method [44]. An eight-layered perfectly matched layer (PML) was used at the boundaries of the computational domain to simulate propagation in an infinite free space and avoid spurious reflections. The dielectric response of gold was represented by Johnson and Christy's parameters (based on experimental data) [45,46]. A conformal mesh was used in all simulations to improve the representation of interfaces of different dielectric materials. The convergence of results was checked with respect to the number of PML layers, size of the computational window, conformal mesh type and mesh accuracy. A change less than 0.2% in Q and a stable value of the resonant wavelength (less than 1 nm change) was observed with the parameters selected for the simulations. To study the resonant modes and their corresponding Qs, a narrow temporal Gaussian pulse was used as the excitation field for both the point source and the waveguide. In order to capture the mode profiles and field patterns, discrete Fourier transforms (DFT) of the electromagnetic field components at each resonant mode were computed on the mesh points while the simulations are running. The Q of the structure was determined from the slope of the decaying field at the resonant frequency [47]. The evaluation of V_{eff} was performed as described in Kristensen *et al.* [3], where the total energy in the device is normalized to the maximum intensity in the device. The intensity ratio, R_i , the ratio between

the optical intensities at the centers of the BNA gap and the PhC cavity was obtained by calculating DFT of the electromagnetic field at the centers of the BNA gap and PhC cavity.

4. Figure of merit

In order to optimize the hybrid resonator for multiplexed arrays of single-molecule experiments, the energy in the externally accessible hot-spot in the BNA gap, U_{BNA} , must be maximized for a given input power, P_{in} . This leads to the definition of a new figure of merit,

$$FOM = \frac{U_{BNA}}{P_{in}}, \quad (1)$$

From the definition of Q (using time-reversal symmetry), the input power is,

$$P_{in} = \frac{2\pi f_{opt} U_{hybrid}}{Q}, \quad (2)$$

where f_{opt} is the fundamental resonant frequency and U_{hybrid} is the energy stored in the hybrid device. Therefore,

$$FOM = \frac{U_{BNA} Q}{2\pi f_{opt} U_{hybrid}}. \quad (3)$$

In the case where most of the energy in the device is stored in the PhC (including the spacer layer),

$$\frac{U_{BNA}}{U_{hybrid}} \approx \frac{V_{BNA} \epsilon_{BNA} E_{BNA}^2}{V_{PhC} \epsilon_{PhC} E_{PhC}^2}, \quad (4)$$

where V_{BNA} and V_{PhC} are the volumes of the BNA gap and the PhC(including the spacer layer) and $\epsilon_{BNA} E_{BNA}^2$ and $\epsilon_{PhC} E_{PhC}^2$ are the maximum energy densities in the BNA hot-spot and PhC cavity, respectively. Once the BNA and PhC cavity designs are fixed, their effective volumes remain nearly constant, so that

$$\frac{U_{BNA}}{U_{hybrid}} \approx \frac{V_{BNA}}{V_{PhC}} R_I, \quad (5)$$

where R_I is the ratio of the optical intensities at the centers of the BNA gap and the PhC cavity, respectively. Thus, the figure of merit becomes:

$$FOM \approx \frac{V_{BNA} R_I Q}{2\pi f_{opt} V_{PhC}} \propto R_I Q. \quad (6)$$

Therefore having fixed the separate PhC cavity and BNA designs, we need only to optimize the product $R_I Q$ when designing the spacer layer. This shows that the performance of the device can be improved by starting with a PhC cavity with a high Q/V ratio. Once the designs of the individual components are fixed, the overall structure combining the BNA and PhC cavity can be optimized by maximizing $R_I Q$. Equation (6) also shows that the FOM increases with decreasing reservoir volume, V_{PhC} .

This new figure of merit represents an important departure from the use of V_{eff} and Q/V_{eff} , which are commonly used to optimize and compare the designs of simple (i.e. non-hybrid) resonators. V_{eff} is normally calculated by dividing the total energy in the resonator by the maximum optical intensity [3]. This method systematically underestimates the mode volume of the resonator, because it implicitly assumes that the optical intensity in the cavity is the

same as the peak intensity. At the same time, however, it eliminates the difficulty of defining the mode boundaries and greatly simplifies the calculation. However, applying this method of calculating V_{eff} to a hybrid photonic-plasmonic cavity is physically misleading and can give V_{eff} anomalous intensity dependence. This is due to the very high intensity in the plasmonic nanoantenna, which is strongly localized so that only a relatively small percentage of the total energy is stored there ($< 2\%$ for the device proposed here—refer to Figs. 4b, 5b). Consequently, V_{eff} for the hybrid resonator often appears to be much smaller than the actual volume in which most of the energy in the device is stored (i.e. the PhC cavity). A misleading value for V_{eff} also affects the value of Q/V_{eff} , which seeks to provide a measure of how tightly the energy in the structure is confined spatially and spectrally. Furthermore, Q/V_{eff} does not consider where the optical localization takes place and gives no measure of the energy, which is actually accessible externally. Thus, although calculated and presented here for comparison with other work in the field, the values of V_{eff} and Q/V_{eff} should be treated with care.

5. Optimization of the spacer layer

The spacer layer is optimized by changing its thickness and structure. The optimization of the spacer thickness for the proposed hybrid resonator is shown in Fig. 2. All the simulations are performed for the fundamental mode of the hybrid device. When the BNA sits directly on top of the PhC cavity ($d = 0$ nm), R_t is at its highest and a large proportion of the energy ($U \propto E^2$) is dissipated by the BNA (Fig. 2(a)) causing the energy efficiency to be at its lowest with $Q = 817$ (Fig. 2(b)). Thus, even though the light in the resonator is strongly coupled to the BNA resulting in a high R_t , the actual optical intensity in the hot-spot is low because the total energy stored in the device is low. When $d = 0$, the effective mode volume also has its lowest value of $V_{eff} = 0.059 ((\lambda/n)^3)$, as shown in Fig. 2(c), and Q/V_{eff} is 13,850. This is because of the low stored energy and the comparatively high intensity in the BNA gap. As d increases to 150 nm, the energy loss from the BNA decreases and the Q of the resonator increases, reaching a maximum of 26,000 at $d = 150$ nm (Fig. 2(b)). As d increases beyond 150 nm, the SiO_2 layer begins to act like a semi-infinite optical cladding layer and the optical field in the BNA becomes insignificant. At the same time, the Q of the resonator drops due to an increase in the effective membrane thickness. Extending the holes of the PhC into the SiO_2 spacer reduces losses due to waveguiding in the spacer, thereby increasing Q up to three folds (Fig. 2(b)). Although Q/V_{eff} is largest for $d = 150$ nm, R_t is low (Fig. 2(a)). The spacer thicknesses which minimizes V_{eff} at $d = 0$ nm or maximizes Q/V_{eff} at $d = 150$ nm, both lead to suboptimal performance i.e. low values of R_tQ as shown in Fig. 2(e). In terms of the new FOM, R_tQ , the best performance is obtained for a spacer thickness of $d = 75$ nm, which gives $\text{FOM} \propto R_tQ \sim 35,000$. This design provides significant optical intensity enhancement in the externally accessible BNA gap while maintaining high optical efficiency or Q . For this design, the optical intensity at the center of the BNA gap is 4.3 times higher than that at the center of the PhC cavity and $Q = 8,200$. This demonstrates the importance of the new figure of merit and shows that the highest field intensity in the BNA gap for a given input power is obtained with spacer thickness of 75 nm.

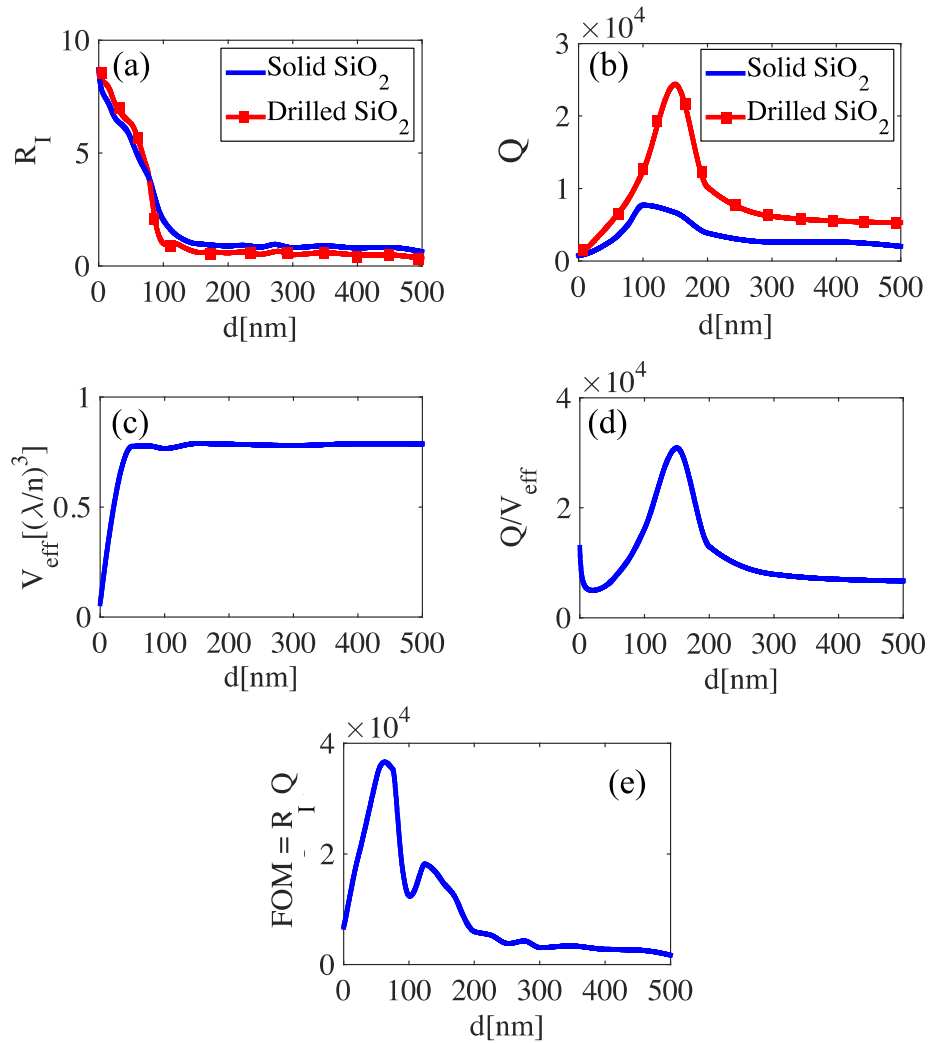


Fig. 2. Effect of changing the spacer layer thickness, d , on the (a) Q , (b) R_I , (c) V_{eff} , (d) Q/V_{eff} and (e) $R_I Q$. Figures are produced at the fundamental resonant mode of the structure.

6. Characteristics of the optimized hybrid device

6.1 Spectral response

The spectral responses of the isolated BNA, isolated L3 PhC cavity and hybrid device are presented in Fig. 3. The hybrid device has a spectral response similar to that of the PhC cavity and sharper than the spectral response of the isolated BNA with a fundamental resonant mode at $\lambda_0 = 1.54 \mu\text{m}$ and second resonant mode at $\lambda = 1.36 \mu\text{m}$. The resonant mode of the isolated PhC cavity at $\lambda = 1.47 \mu\text{m}$ is not present in the hybrid structure because its field distribution has a zero at the center of the cavity. Thus, it does not get resonantly enhanced by the BNA in the hybrid device. As expected, the spectral response of the hybrid structure is identical irrespective of whether it is evaluated in the PhC cavity, the spacer layer or the BNA gap.

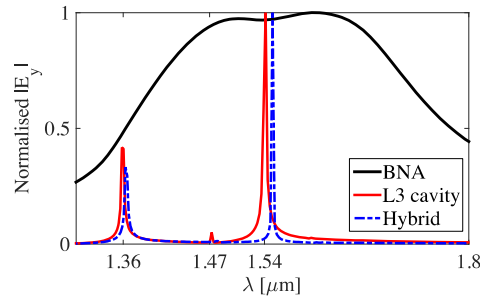


Fig. 3. Comparison between the spectral responses of the isolated L3 cavity (red curve), the hybrid nanoresonator comprised of the BNA and the L3 PhC cavity separated by a 75nm thick drilled layer of SiO₂ (blue dashed curve) and the 700nm BNA placed on top a 75nm thick layer with an effective reflective index matching the PhC layer and the SiO₂ layer (black curve). The curves are normalized with respect to their maximum value.

6.2 Intensity profiles

Figures 4(a-d) show the optical intensity distribution ($|E_y|^2$) in the xy and yz planes passing through the center of the device with and without the BNA excited with a point source at the centre of the PhC cavity. Figure 4(e) shows the optical intensity ($|E_y|^2$) along a vertical line passing through the center of the structures with and without the BNA when the structure. The values of intensity throughout the devices are normalized with respect to the intensity at the center of the PhC cavity. Comparing the optical intensity distributions for the devices with and without the BNA are presented in Figs. 4 (b,d) and Figs. 4(a,c). It is clear that presence of the BNA creates an externally accessible hot-spot in the BNA gap and suppresses the optical field where the metal is located, resulting in high intensity gradients at the BNA gap. This is essential for optical trapping and manipulation experiments. As seen in Fig. 4(e), the optical intensity on top of the structure (at the position of the BNA gap) is approximately 60 times larger when the BNA is present.

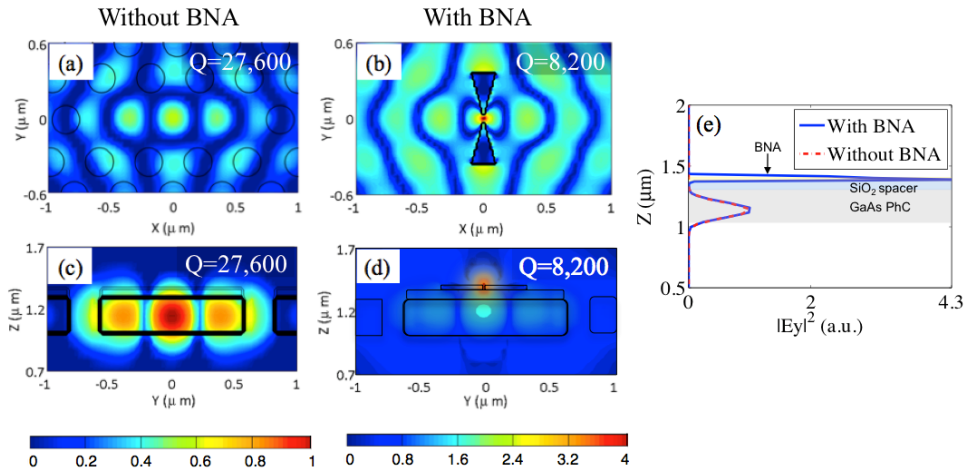


Fig. 4. Logarithmic plots of the optical intensity ($|E_y|^2$) in the xy plane positioned on the top surface of the structures (including the 75 nm thick spacer layer) (a) without and (b) with the BNA and in the yz plane passing through the center of the structure (c) without and (d) with the BNA when the structure is excited with a point source. (e) Shows the comparison of the optical intensity ($|E_y|^2$) along a vertical line passing through the center of the structure with (blue) and without (red) the BNA when the structure is excited with a point source.

The structure was then excited using a W1 waveguide to demonstrate its suitability for planar photonic integration. In this case, similar to when excited with a point source, an

externally accessible hot-spot is created at the BNA gap as shown in Fig. 5(a). Figure 5(b) shows the optical intensity ($|E_y|^2$) along a vertical line passing through the center of the structures with and without the BNA. The optical intensity in each simulation is normalized with respect to the power transferred from the waveguide to the hybrid cavity. This is calculated by subtracting the total power exiting through the waveguide from the total power entering through the waveguide. The optical intensity on top of the structure (at the position of the BNA gap) is 40 times larger when the BNA is present compared to when it is not.

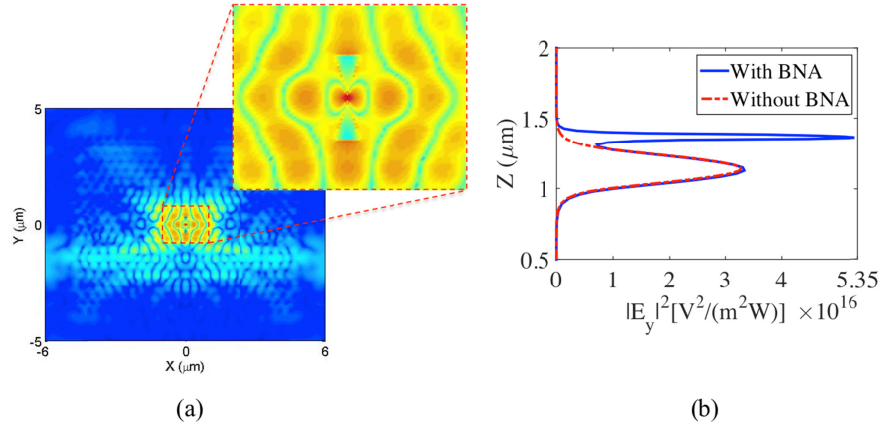


Fig. 5. (a) Logarithmic plot of the optical intensity ($|E_y|^2$) in the xy plane at the top surface of the structure when the hybrid cavity is excited via a W1 PhC waveguide. (b) The expanded plot shows the optical intensity pattern in the BNA region. Comparison of the optical intensity ($|E_y|^2$) along a vertical line passing through the center of the structure with (blue) and without (red) the BNA when the structure is excited with a W1 waveguide.

When coupling light into the hybrid device using the W1 waveguide, the S_{21} parameter (forward gain in the optical field) is set to -0.76dB for the fundamental resonant mode of the hybrid device. Thus approximately 17% of the input light in the waveguide couples into a single hybrid device, making its excitation very energy efficient compared to structures comprised of arrays of metallic nanoantennas illuminated vertically. When arrays of nanoplasmonic antennas are used (as opposed to a hybrid photonic-plasmonic device), the laser light goes through lossy optics and the light at the BNA gap reaches enhancements up to 10 times the incident intensity. In the proposed hybrid device, we can achieve optical intensities in the BNA gap 60 times higher than the optical intensity on top of the PhC cavity.

7. Overall comparison

Table 1 provides a comparison between the characteristics of the hybrid device and its individual components. The hybrid structure has a higher Q compared to the isolated BNA and a lower V_{eff} compared to the isolated PhC cavity. The isolated PhC cavity has a higher Q/V_{eff} compared to the hybrid structure, but does not provide an externally accessible hot-spot and therefore would not be suitable for studying single-molecule interactions. This is a good example of why the merit of certain devices should not be determined by considering Q/V_{eff} alone. R_1 and R_1Q are also quoted for the two PhC resonator structures in Table 1 for comparison. R_1 is simply the ratio of the intensity at the surface to that at the center of the cavity in these cases.

Table 1. Comparison of λ_0 , Q, V_{eff} , Q/V_{eff} and R_1Q of the device at different design stages.

Structure	λ_0	Q	V_{eff} $((\lambda/n)^3)$	R_1	Q/V_{eff}	R_1Q
Isolated BNA	1.35	25	0.0033	-	7,500	-
Isolated PhC L3	1.54	39,500	0.778	0.65	50,700	25,675
PhC L3 + 75nm drilled spacer	1.54	27,600	0.787	0.028	35,000	770
Hybrid device	1.55	8,200	0.777	4.3	10,500	35,000

8. Discussions

We envisage the development of hand-held, application-specific platforms with highly integrated arrays of hybrid optical resonators. Such platforms would produce patterns of nano-sized optical hot-spots on a smooth surface and be illuminated and interrogated via a hidden network of waveguides. The successful realization of this platform will contribute to advances in many fields, including chemistry, life sciences, personalized medicine and quantum information technology.

The ability of the hybrid resonator to trap on the nanoscale allows individual molecules and nanoparticles to be controlled and studied. The BNA hot-spot in the hybrid device has approximately 40 times higher intensity than the evanescent field at the surface of a conventional PhC cavity. Furthermore, the intensity gradient is as important as the intensity and enters directly into the Maxwell stress tensor describing optical forces. The high intensity in the BNA gap and nanoscale localization produce very large intensity gradients around the hot-spot, including a positive vertical gradient, which eliminates the force drawing trapped particles down onto the PhC surface and replaces it with an upward force drawing the particles back into the hot-spot. At the same time, when the hybrid resonator is pumped through a waveguide, it only delivers light to the BNA and suppresses the unwanted illumination of the specimen across the rest of the surface. For the region without the BNA, the SiO₂ spacing layer further reduces the surface evanescent field of the waveguides, offering additional control over the parasitic trapping and guiding of particles.

Conventional optical manipulation and nanoplasmonic trapping setups are very energy inefficient where most of the light is lost passing through the bulk optics or by illuminating a large proportion of the glass substrate rather than just the BNAs. The ability to couple the hybrid resonator to an optical waveguide is a key attribute of this device, which greatly improves its efficiency and allows the unused energy to be used by devices downstream. The coupling between the waveguide and the hybrid device can be controlled by tailoring the design of the waveguide and its distance from the cavity to adjust the number of hybrid devices that can be powered and characterized using a single waveguide. Using the W1 waveguide design in this paper, about 16% of the input light is coupled into the hybrid cavity, about 2% of which is concentrated in the BNA hot-spot. By properly engineering the waveguide-cavity coupling coefficients, this waveguide could support the uniform excitation of four hybrid cavities.

The resonances of the devices can be individually tuned by small changes to the PhC cavity. Thus, light can be selectively delivered to specific resonators by tuning the excitation to the appropriate wavelength, allowing unprecedented control over the optical potential surface of the sample and making it possible to perform many different (or identical) single molecule experiments simultaneously. By facilitating parallel experiments, the platform will reduce the time and effort needed to collect enough data to draw statistically valid conclusions. At the same time, it will reduce the cost, time and complexity of the experiments, while simultaneously increasing experimental control and accuracy.

Finally, as a highly integrated, fiber-connected platform, it will be simple and ideal for coupling to micro- and nanofluidic systems for the delivery of the molecules and particles and bespoke optical interrogation systems based on photonic integrated circuits. The flat surface

of this device will minimize the unintended adhesion of molecules to morphological surface features and simplify the use of surface treatments and application specific coatings.

9. Summary and conclusions

This paper addresses the design of a hybrid photonic-plasmonic resonator as the key building block of a multicomponent platform for high-throughput, single-molecule experiments. The hybrid device is comprised of an L3 PhC cavity coupled to a BNA, with a SiO₂ layer separating the BNA from the PhC cavity. By defining a new FOM that is more appropriate for our target application, the thickness of the spacer layer is optimized to maximize the energy in the BNA gap for a given input power. The device produces an externally accessible hot-spot, whose intensity is 40–60 times larger than that of the evanescent field at the surface of an isolated PhC cavity and at least 4.3 times larger than the intensity at the center of the PhC cavity. The optical intensity gradient (often a more important parameter than the optical intensity) created around the hot-spot in the BNA gap will contribute significantly to its trapping performance for nanoparticles. Finally, the hybrid resonator can be excited via a PhC waveguide, greatly improving its energy efficiency and making it compatible with user-friendly fiber-optic and photonic integrated circuit technologies. Thus, when successfully fabricated, this hybrid resonator will allow the realization of an integrated platform suitable of conducting a large number of single-molecule experiments simultaneously.

Funding

Engineering and Physical Sciences Research Council [grant number EP/H024891/1].

Acknowledgements

This work was supported by the Engineering and Physical Sciences Research Council [grant number EP/H024891/1]. M. Mossayebi gratefully acknowledges the support of the University of Nottingham under the Dean of Engineering scholarship for international excellence and the Building Experience and Skill Travel Scholarships.

References

1. K. C. Neuman and A. Nagy, "Single-molecule force spectroscopy: optical tweezers, magnetic tweezers and atomic force microscopy," *Nat. Methods* **5**(6), 491–505 (2008).
2. K. C. Neuman and S. M. Block, "Optical trapping," *Rev. Sci. Instrum.* **75**(9), 2787–2809 (2004).
3. P. T. Kristensen, C. Van Vlack, and S. Hughes, "Generalized effective mode volume for leaky optical cavities," *Opt. Lett.* **37**(10), 1649–1651 (2012).
4. J. A. Schuller, E. S. Barnard, W. Cai, Y. C. Jun, J. S. White, and M. L. Brongersma, "Plasmonics for extreme light concentration and manipulation," *Nat. Mater.* **9**(3), 193–204 (2010).
5. A. Kinkhabwala, Z. Yu, S. Fan, Y. Avlasevich, K. Müllen, and W. Moerner, "Large single-molecule fluorescence enhancements produced by a bowtie nanoantenna," *Nat. Photonics* **3**(11), 654–657 (2009).
6. M. L. Juan, M. Righini, and R. Quidant, "Plasmon nano-optical tweezers," *Nat. Photonics* **5**(6), 349–356 (2011).
7. B. J. Roxworthy, K. D. Ko, A. Kumar, K. H. Fung, E. K. Chow, G. L. Liu, N. X. Fang, and K. C. Toussaint, Jr., "Application of plasmonic bowtie nanoantenna arrays for optical trapping, stacking, and sorting," *Nano Lett.* **12**(2), 796–801 (2012).
8. N. A. Hatab, C. H. Hsueh, A. L. Gaddis, S. T. Retterer, J. H. Li, G. Eres, Z. Zhang, and B. Gu, "Free-standing optical gold bowtie nanoantenna with variable gap size for enhanced Raman spectroscopy," *Nano Lett.* **10**(12), 4952–4955 (2010).
9. J. N. Anker, W. P. Hall, O. Lyandres, N. C. Shah, J. Zhao, R. P. Van Duyne, "Biosensing with plasmonic nanosensors," In *Nanoscience And Technology: A Collection of Reviews from Nature Journals*, 308–319 (2010).
10. P. Mestres, J. Berthelot, S. S. Aćimović, and R. Quidant, "Unraveling the optomechanical nature of plasmonic trapping," *Light Sci. Appl.* **5**(7), e16092 (2016).
11. Y. Pang and R. Gordon, "Optical trapping of a single protein," *Nano Lett.* **12**(1), 402–406 (2012).
12. J. D. Joannopoulos, P. R. Villeneuve, and S. Fan, "Photonic crystals: putting a new twist on light," *Nature* **386**(6621), 143–149 (1997).
13. G. Magno, M. Fevrier, P. Gogol, A. Aassime, A. Bondi, R. Mégy, and B. Dagens, "Strong coupling and vortexes assisted slow light in plasmonic chain-SOI waveguide systems," *Sci. Rep.* **7**(1), 7228 (2017).
14. D. Conteduca, F. Dell'Olio, T. F. Krauss, and C. Ciminelli, "Photonic and plasmonic nanotweezing of nano- and microscale particles," *Appl. Spectrosc.* **71**(3), 367–390 (2017).

15. M. Kamandar Dezfouli and S. Hughes, "Quantum optics model of surface-enhanced Raman spectroscopy for arbitrarily shaped plasmonic resonators," *ACS Photonics* **4**(5), 1245–1256 (2017).
16. E. Bermúdez-Ureña, G. Tutuncuoglu, J. Cuerda, C. L. C. Smith, J. Bravo-Abad, S. I. Bozhevolnyi, A. Fontcuberta I Morral, F. J. García-Vidal, and R. Quidant, "Plasmonic Waveguide-Integrated Nanowire Laser," *Nano Lett.* **17**(2), 747–754 (2017).
17. F. Todisco, M. Esposito, S. Panaro, M. De Giorgi, L. Dominici, D. Ballarini, A. I. Fernández-Domínguez, V. Tasco, M. Cuscunà, A. Passaseo, C. Ciraci, G. Gigli, and D. Sanvitto, "Toward cavity quantum electrodynamics with hybrid photon gap-plasmon states," *ACS Nano* **10**(12), 11360–11368 (2016).
18. M. Bahramipani, S. Dutta-Gupta, B. Abasahl, and O. J. F. Martin, "Cavity-Coupled Plasmonic Device with Enhanced Sensitivity and Figure-of-Merit," *ACS Nano* **9**(7), 7621–7633 (2015).
19. S. Cui, X. Zhang, T. Liu, J. Lee, D. Bracher, K. Ohno, D. Awschalom, and E. L. Hu, "Hybrid plasmonic photonic crystal cavity for enhancing emission from near-surface nitrogen vacancy centers in diamond," *ACS Photonics* **2**(4), 465–469 (2015).
20. S. Mokkapati, D. Saxena, N. Jiang, L. Li, H. H. Tan, and C. Jagadish, "An order of magnitude increase in the quantum efficiency of (Al)GaAs nanowires using hybrid photonic-plasmonic modes," *Nano Lett.* **15**(1), 307–312 (2015).
21. M. Castro-Lopez, N. de Sousa, A. Garcia-Martin, F. Y. Gardes, and R. Sapienza, "Scattering of a plasmonic nanoantenna embedded in a silicon waveguide," *Opt. Express* **23**(22), 28108–28118 (2015).
22. Y. Luo, M. Chamanzar, A. Apuzzo, R. Salas-Montiel, K. N. Nguyen, S. Blaize, and A. Adibi, "On-chip hybrid photonic-plasmonic light concentrator for nanofocusing in an integrated silicon photonics platform," *Nano Lett.* **15**(2), 849–856 (2015).
23. A. El Eter, N. M. Hameed, F. I. Baida, R. Salut, C. Filiatre, D. Nedeljkovic, E. Atie, S. Bole, and T. Grosjean, "Fiber-integrated optical nano-tweezer based on a bowtie-aperture nano-antenna at the apex of a SNOM tip," *Opt. Express* **22**(8), 10072–10080 (2014).
24. Z. Li, J. Kou, M. Kim, J. O. Lee, and H. Choo, "Highly efficient and tailorable on-chip metal–insulator–metal plasmonic nanofocusing cavity," *ACS Photonics* **1**(10), 944–953 (2014).
25. I. Mukherjee and R. Gordon, "Analysis of hybrid plasmonic-photonic crystal structures using perturbation theory," *Opt. Express* **20**(15), 16992–17000 (2012).
26. M. Xi and B. M. Reinhard, "Localized surface plasmon coupling between mid-IR-resonant ITO nanocrystals," *J Phys Chem C Nanomater Interfaces* **122**(10), 5698–5704 (2018).
27. X. Yang, A. Ishikawa, X. Yin, and X. Zhang, "Hybrid photonic-plasmonic crystal nanocavities," *ACS Nano* **5**(4), 2831–2838 (2011).
28. M. Chamanzar and A. Adibi, "Hybrid nanoplasmonic-photonic resonators for efficient coupling of light to single plasmonic nanoresonators," *Opt. Express* **19**(22), 22292–22304 (2011).
29. X. He, L. Yang, and T. Yang, "Optical nanofocusing by tapering coupled photonic-plasmonic waveguides," *Opt. Express* **19**(14), 12865–12872 (2011).
30. R. F. Oulton, V. J. Sorger, D. Genov, D. Pile, and X. Zhang, "A hybrid plasmonic waveguide for subwavelength confinement and long-range propagation," *Nat. Photonics* **2**(8), 496–500 (2008).
31. A. L. Pyayt, B. Wiley, Y. Xia, A. Chen, and L. Dalton, "Integration of photonic and silver nanowire plasmonic waveguides," *Nat. Nanotechnol.* **3**(11), 660–665 (2008).
32. F. De Angelis, M. Patrini, G. Das, I. Maksymov, M. Galli, L. Businaro, L. C. Andreani, and E. Di Fabrizio, "Nanoscale chemical mapping using three-dimensional adiabatic compression of surface plasmon polaritons," *Nano Lett.* **8**(8), 2321–2327 (2008).
33. M. Barth, S. Schietinger, S. Fischer, J. Becker, N. Nüsse, T. Aichele, B. Löchel, C. Sönnichsen, and O. Benson, "Nanoassembled plasmonic-photonic hybrid cavity for tailored light-matter coupling," *Nano Lett.* **10**(3), 891–895 (2010).
34. T. Zhang, S. Callard, C. Jamois, C. Chevalier, D. Feng, and A. Belarouci, "Plasmonic-photonic crystal coupled nanolaser," *Nanotechnology* **25**(31), 315201 (2014).
35. A. E. Eter, T. Grosjean, P. Viktorovitch, X. Letartre, T. Benyattou, and F. I. Baida, "Huge light-enhancement by coupling a Bowtie Nano-antenna's plasmonic resonance to a photonic crystal mode," *Opt. Express* **22**(12), 14464–14472 (2014).
36. M. Mossayebi, G. Bellanca, A. Parini, A. J. Wright, and E. C. Larkins, "Engineering of Hybrid Photonic-Plasmonic Devices for Enhanced Light-Matter Interactions," In *Recent Trends in Computational Photonics*, Springer, Cham., 369–390 (2017).
37. M. Mossayebi, A. J. Wright, A. Parini, M. G. Somekh, G. Bellanca, and E. C. Larkins, "Investigating the use of a hybrid plasmonic–photonic nanoresonator for optical trapping using finite-difference time-domain method," *Opt. Quantum Electron.* **48**(5), 275 (2016).
38. F. Zhang, J. Ren, X. Duan, Z. Chen, Q. Gong, and Y. Gu, "Evanescent-field-modulated two-qubit entanglement in an emitters-plasmon coupled system," *J. Phys. Condens. Matter* **30**(30), 305302 (2018).
39. C. Ciminelli, D. Contedduca, F. Dell'Olio, and M. Armenise, "Design of an optical trapping device based on an ultra-high Q/V resonant structure," *IEEE Photonics J.* **6**(6), 1–16 (2014).
40. C. Sauvan, P. Lalanne, and J. P. Hugonin, "Slow-wave effect and mode-profile matching in photonic crystal microcavities," *Phys. Rev. B Condens. Matter Mater. Phys.* **71**(16), 165118 (2005).

41. W. Yu-Ming, L. Le-Wei, and L. Bo, "Geometric effects in designing bow-tie nanoantenna for optical resonance investigation.", *Electromagnetic Compatibility (AEMC), 2010 Asia- Pacific Symposium on*, 1108–1111 (2010).
42. H. Chen, A. M. Bhuiya, R. Liu, D. M. Wasserman, and K. C. Toussaint, Jr., "Design, fabrication, and characterization of near-IR gold bowtie nanoantenna arrays," *J. Phys. Chem. C* **118**(35), 20553–20558 (2014).
43. S. Malaguti, G. Bellanca, L. Ottaviano, K. Yvind, S. Combrié, A. De Rossi, and S. Trillo, "Tailored design of WDM filters in BCB embedded PhC membranes," *Opt. Quantum Electron.* **45**(4), 329–342 (2013).
44. LumericalSolutions, Inc., <http://www.lumerical.com/tcad-products/fdtd/>.
45. P. B. Johnson and R. W. Christy, "Optical constants of the noble metals," *Phys. Rev. B* **6**(12), 4370–4379 (1972).
46. A. C. Lesina, A. Vaccari, P. Berini, and L. Ramunno, "On the convergence and accuracy of the FDTD method for nanoplasmonics," *Opt. Express* **23**(8), 10481–10497 (2015).
47. https://kb.lumerical.com/en/index.html?diffractive_optics_cavity_q_calculation.html.